Trans. of the Society of Instrument and Conrol Engineers
Vol. E-2, No. 1, 81/90 (2002)

Performance of Three-Finger Multisensory Hand on Spacevehicle "Hikoboshi"

Kazuo Machida*, Yoshitsugu Toda** and Yuichi Murase***

A hand with dexterity and local autonomy is one of the key components of a space robot to perform precise in-orbit servicing. This paper presents performance of the three-finger multisensory hand boarded on the unmanned spacevehicle "Hikoboshi". The hand comprises a newly devised three-finger module with grip force sensors and a wrist compliance device with displacement sensors. It also has a hand-eye camera and three range sensors for non-contact sensing. The contact sensors display fine performance owing to zero-gravity of space compared with the ground. The laser/PSD type proximity range sensors retain performance under the high intensity of sunlight in orbit. Although the hand-eye camera is useful for position measurement of objects through image processing in most case, some points are noticed to use it in satellite daytime owing to intensity and direction variations of sunlight. The robot performed high precision tasks in space utilizing these hand mechanisms and multisensors through sensor-fused telerobotics.

Key Words : Space robot. Multisensory hand. Range sensor. Grip force sensor. Hand eye camera

1. Introduction

As the utilization of space increases, robots performing work replacing that of humans in the dangerous environment outside of spacevehicles are desired. To date, robots that are used outside of spacevehicles have mainly been developed for transporting large cargos and installation/removal of payloads. As an end effecter of these robots, the snare type[1], which holds objects by closing three wires in the shuttle arm, the gripper type[2] in the SPDM (Special Purpose Dexterous Manipulator) of the space station, and the three-nail tool type in the subarm used in the JEMRMS (Japanese Experiment Module Remote Manipulator System) have been used[3),4]. These end effectors have one degree of freedom and are not equipped with sensory functions, thus they are not suitable for precision work. They also require exclusive fixtures on the objects[5]. ROTEX (Robot Technology Experiment) was performed as a precision work robot experiment in a manned spacevehicle[6]. The multisensory hand was used in the ROTEX. However, it can only be used in air-conditioned racks of the Space Lab (Space Laboratory); it cannot be used outside of spacevehicles where the environmental conditions are severe and highly variable. Furthermore, the degree of freedom of the gripper is one, thus there are restrictions such as the requirement of fixtures on the object.

We developed a high-performance robot hand which carries out precision work outside of a spacevehicle[7], and carried out space tests on the Engineering Test Satellite-VII, (Hikoboshi (Altair)), from 1998 to 2000. The features of the robot hand include the capability of performing precision work on various objects by the three-finger multisensory structure, local autonomy, and the capacity to be used outside of a spacevehicle. The hand has multipurpose features that enable it to be fixed to various types of arms, therefore, it has become the world's front-runner hand for performing precision work outside of spacevehicles. The design of the hand has already been published[8]. In this paper, we describe the characteristics of the hand and its performance in space. First, we outline the structure of the hand. We then describe the finger mechanism and a wrist compliance device, as well as the performance of grip force sensors and microdisplacement sensors incorporated into the hand. We also describe the measurement performance of image and range sensors used as non-contact optical sensors. Finally, we report an actual example of a precision task performed by the hand.

2. Three-finger multisensory hand

The first important requirement for the hand used in precision work is that it must have mechanisms which enable it to grasp objects of various shapes securely and to adjust their positions and grip force accurately. The second important requirement is that autonomous characteristics must be improved because of the following reasons: i) the communication link between the ground station and robots in space is not always secure, ii) it is difficult to secure a sufficient communication capacity and iii) there is a large communication delay time. Therefore, improvement of autonomy is required and multiple sensors are indispensable. The

* The University of Tokyo, RCAST, 4-6-1, Komaba Meguro-Ku, Tokyo
** AIST, Tsukuba
*** Fujitsu Laboratories Ltd., Kawasaki

third important issue is related to the accumulation of model errors during a series of tasks because in-orbit services usually require multiple tasks. Therefore, functions such as monitoring the work environment and performing calibrations are important.

Fig. 1 shows a photo of the developed flight model of the three-finger multisensory hand which satisfies the above conditions. The finger mechanism consists of a linear-motion finger which corresponds to our thumb and two rotation fingers, i.e., the middle finger and index finger. We provided one degree of freedom to each finger, made the total degrees of freedom three and gave them versatility to grasp objects. At the same time, we made the fingers perform precision position adjustment and control the grip force. A compliance device was incorporated into the hand in order for the hand to compensate for positional errors and to absorb impacts. A hand-eye camera and laser proximity range sensors as optical sensors, grip force sensors as touch sensors, wrist displacement sensors and force/torque sensors were arranged around the hand. Also, to enable work in the eclipse, a microlight source consisting of LED arrays was installed on the side of the hand. A grapple fixture to enable the connection of various types of robot arms in orbit was installed on the wrist side of the hand. A signal processor for serial conversion of primary signals from the sensors was installed at the central section of the hand. Calibration of sensors such as the range sensors which are affected by temperature was carried out by installing a thermistor on the signal processing board to improve the measurement accuracy. The robot controls process and makes judgments necessary for carrying out precision work using these sensors.**Table 1** lists the specifications of these sensors.

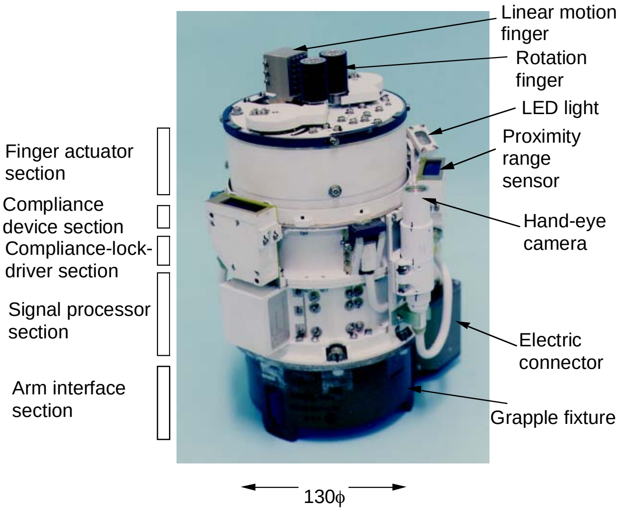

Fig.1 Flight model of three-finger multisensory hand

Table 1 Specifications of hand sensors

Sensors	Specifications
Grip force sensor	Range: 0.7~25N Accuracy: ±0.7N
Wrist displacement sensor	Range: ±1.5mm (x, y) ±2deg (θz) Accuracy: ±0.05mm (x, y) ±0.1deg (θz)
Force/torque sensor	Range: 50N (Fx, Fy), 100N (Fz) 4.9Nm (Mx, My, Mz) Linearity: 0.4%
Proximity range sensor	Range: 0~80mm Accuracy: ±1mm Misalignment allowance: 25deg
Hand eye camera	Field of view: 85x64mm Resolution: 0.14mm (at 40mm distance)

The hand is usually connected to a 0.5-m-long arm (repetitive positioning accuracy: 0.3 mm) and performs precision task experiments. It can also be connected to a 2.4-m-long arm developed by the National Space Development Agency of Japan (NASDA) and we performed experiments on docked satellite "Orihime (Vega)" [7]. **Fig. 2** shows an image near the hand on "Hikoboshi" which was received from satellite. Various work components are installed on a task board shown on the right-hand side of the picture. The altitude of the satellite orbit is 550 km, the inclination angle is 35 deg, and the robot is mounted on the surface of the satellite facing the earth. In Fig. 2, the lower part of the photo is the side on which the robot is mounted, and the earth is located above the area shown in the photo. Therefore, the satellite receives sunlight directly from the side in the morning and during sunset. During daytime, the sunlight reflected by the earth (albedo) illuminates the satellite from the upper direction with respect to the photo. Since the period of time in which it takes a satellite to complete an orbital trip is approximately 96 min, the lighting condition changes 15-fold faster than that on the earth. The temperature around the arm was measured to be from -35°C to +25°C.

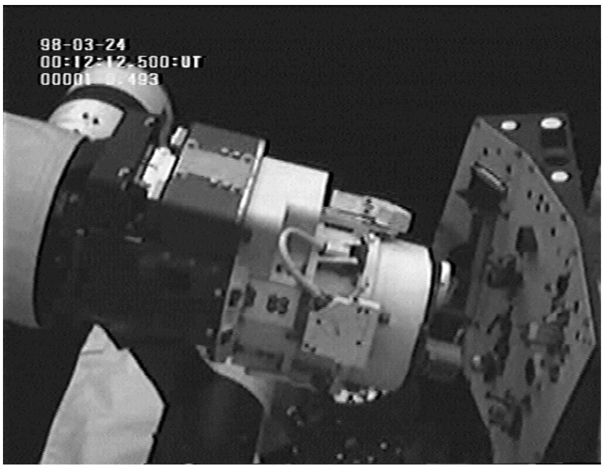

Fig.2 View of hand in orbit

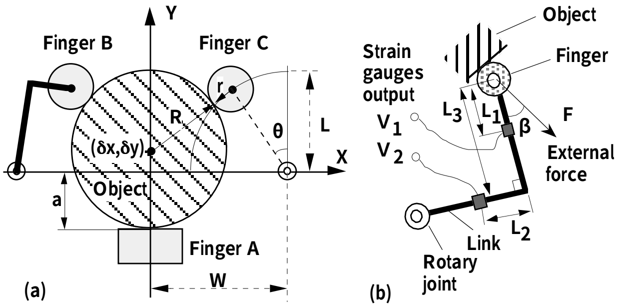

Fig.3 Schematics of finger module (a: Finger arrangement, b: Grip force sensor)

3. Hand mechanism and force sensing

3.1 Finger module and grip force sensor

Fig. 3 shows a schematic diagram of the finger mechanics. The hand is designed to grasp square-shaped objects, sheets, cylinders, polygonal columns and spheres using a linear-motion finger, A, and rotation fingers B and C. A DC brushless motor was used to drive the linear-motion finger, and a pair of stepping motors was used for the rotation fingers to ensure compact device size. Compared with the multijoint fingers, this three-finger mechanism has the following features; i) the structure is simple, highly reliable and can be controlled easily, and ii) compared with single gripper mechanisms, this system can grasp objects of many different shapes and the flexibility of positioning adjustment is excellent. In order to grasp an object, first, the rotation fingers B and C are operated in the “closing” direction. When either of the fingers touches the object, the finger motion is terminated and then the linear-motion finger is closed to grasp the object. After grasping the object, the rotation fingers are operated in the position-control mode and the linear-motion finger is operated in the force-control mode in which the force acting on the rotation fingers is fed back to the linear actuator. A fitting mechanism, consisting of a matrix of pins precompressed by springs, is incorporated in the pad of the linear-motion finger, increasing the grasping stability by making the finger accommodate itself to the shape of the object.

As shown in Fig. 3, strain gauges attached to the L-shaped links of the rotation fingers detect the pressure on the rotation fingers. The strain gauges detect two orthogonal bending moments which act on the links. The detected voltages of the strain gauges, V_1 and V_2 are

$$V_1 = k_1 L_1 F \sin\beta \tag{1}$$

$$V_2 = k_2 L_2 F \cos\beta + k_3 L_3 F \sin\beta \tag{2}$$

Here, K_1, L_1 and β are the output characteristic coefficient, moment arm length and contact angle of the rotation finger, respectively. By obtaining the vertical force F from Eqs. (1) and (2),

$$F = \frac{\sqrt{(k_2 L_2 V_1)^2 + (k_1 L_1 V_2 - k_3 L_3 V_1)^2}}{k_1 k_2 L_1 L_2} \tag{3}$$

The isotropic contact force can be measured using this approach, and it is possible to measure and control grip forces for various objects. Also, the rotation finger can be used for the application of force with high accuracy.

After launching the robot into space, we examined grip force control characteristics of the finger and pressure sensor characteristics. **Fig. 4** shows the grip force control characteristics when an equilateral triangle column was grasped. Here, approximately 20 sec after the start of closing operation of rotation fingers B and C, they made contact with the object. Then, the preset grip force (7.5 N and 15 N) was applied by the closing of finger A. The grip force is controlled without any practical problems. The external force applied to the object at the time of contact was approximately 2 N; it is demonstrated that grasping at low stress, which is an advantage of the use of the fingers with the grip force sensors, is established.

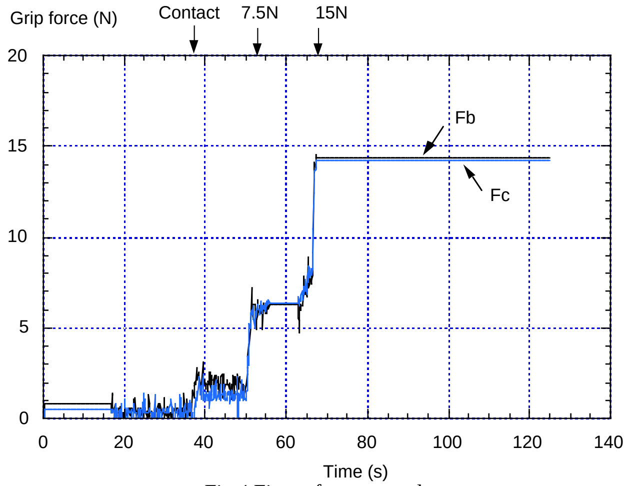

Fig.4 Finger force control

The position sensors and grip force sensors in the finger mechanism are also used for the determination of shapes and positions of objects. When an object to be grasped is a cylinder, letting the rotation angle of the rotation finger C be θ and the opening of the linear finger be a, the radius of the cylinder is given by the following equation from the geometrical relationship (refer to Fig. 3 (a) for symbols).

$$R = \frac{a^2 + L^2 + W^2 - r^2 + 2aL\cos\theta - 2LW\sin\theta}{2(a + r + L\cos\theta)} \tag{4}$$

Also, the deviation of the cylindrical center (δx, δy) with respect to the center of the hand is

$$\delta x = W - L\sin\theta - \lambda(R + r)$$
$$\delta y = R - a \tag{5}$$

where

$$\lambda = \sqrt{1 - \left(\frac{R - a - L\cos\theta}{R + r}\right)^2} \tag{6}$$

A similar relationship can be obtained from the joint angle of rotation finger B (however, the sign on the right-hand side of δx in Eq. (5) is reversed). Accordingly, it is possible to obtain the relative position of the center of the cylinder with respect to the center of the hand from the opening a of linear-motion finger A, and the angle θ of one of the rotation fingers. The driving resolutions of the linear-motion finger and rotation fingers are better than 3 mm and 60 mm, respectively, thus, measurements are possible with the accuracy better than 1 mm even if other error factors are included.

Fig. 5 shows an example of remote measurement. Since the workpiece (hexagonal column) is located outside the view of the monitor camera, we cannot actually see it. In Fig. 5, the workpiece and fingers were displayed by CG via the CAD model of the ground simulator. The fingers are depicted using the telemetry data (a, θ_b, θ_c, and the position of the hand center) transmitted from the satellite. The shape of the finger in Fig. 5(a) shows that this workpiece was held with bias at first, however, it was speculated that this was caused by CAD position data errors. Prompted by this finding, we obtained the deviation using the above equations and confirmed the position once again by regrasping the component after rough calibration (b). Using thus-obtained data, we improved the CAD model and finally completed detailed corrections (c). After these corrections, matching between "the real world," on-board control system and on-ground simulator was performed, leading to smooth operation of subsequent precision work.

3.2 Wrist compliance device and microdisplacement sensor

As shown in **Fig. 6**, a component to support the finger mechanism module by a plate spring was adopted for the wrist compliance device. The prominent feature of this component unlike other components such as RCC (Remote Center Compliance device) is that it is thin and lockable. By successively connecting two pairs of plate springs in a rectangular form, compliance in the x, y and θ_Z directions was applied to the wrist. This is mainly used to absorb horizontal errors during insertion work. Also, two pairs of clover-shaped plate springs were installed to apply compliance in the z direction. These are used to absorb errors and impact in the vertical direction; in addition, they are used as stretch margin of 2mm to confirm completion of a

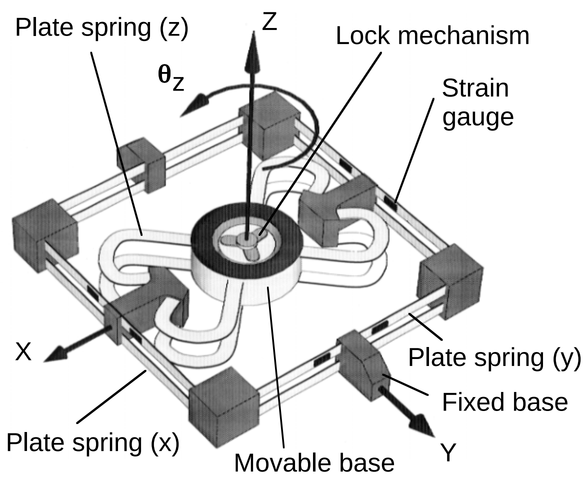

Fig.6 Schematic of wrist compliance device with lock mechanism

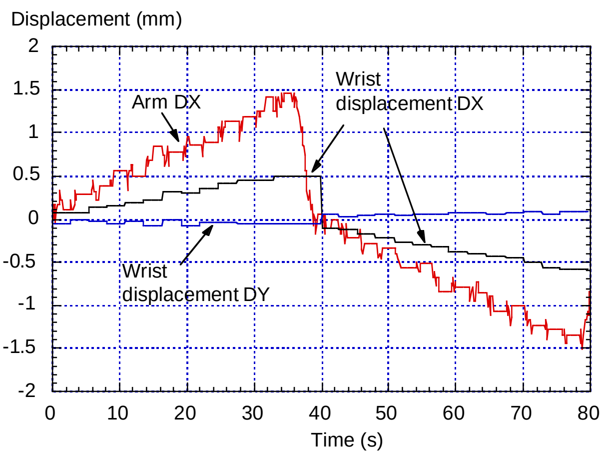

Fig.7 Characteristics of wrist displacement sensor

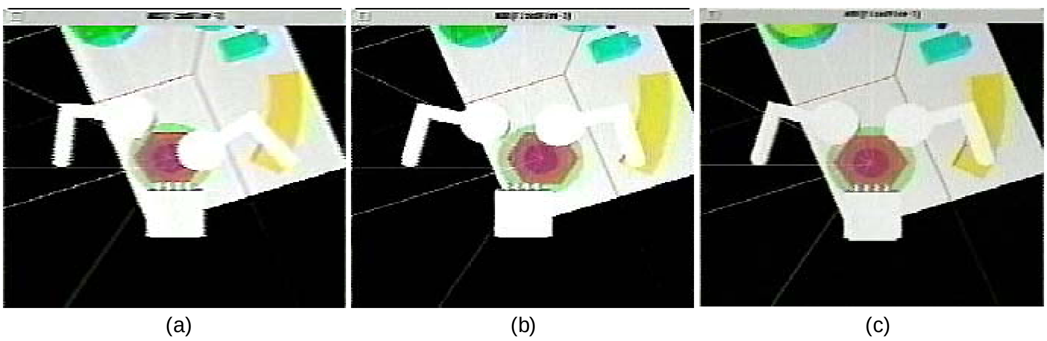

Fig.5 Remote measurement of object position by grasp-sensing from the ground (a: Initial grasping, b: 2nd grasp-sensing, c: Grasping after CG calibration)

connection task by pulling the workpiece. The design values of compliance were 0.15 mm/N in the x and y directions, 0.075 mm/N in the z direction and 3 deg/Nm in the θ_Z direction. A rotating locking mechanism was installed at the center of the movable base; the wrist was capable of taking two states, i.e., soft and stiff states.

Microdisplacement of the wrist was detected by strain gauges attached on plate springs of the compliance device. Since a device which directly tests these sensors is not mounted on the satellite, the sensors were indirectly tested by moving the tip of the arm while a fixed workpiece is grasped and comparing the output with the values obtained by the on-ground tests.**Fig. 7** shows the data when a micromovement in the x direction was carried out by the tip of the arm. The wrist displacement detected was in proportion to the amount of arm-tip displacement. No interference was observed in the y direction (DY). In this testing method, due to the grasping stiffness of the fingers and the effects of displacement of the plate spring in the z direction caused by the moment generated in the wrist, only one-third of the actual arm-tip displacement is detected. Nonetheless, this result agrees with that obtained by the test conducted on the ground, and hence we consider that the sensor characteristics are retained in space.

On the ground, the compliance device has an offset value which depends on the arm joint angle caused by gravity, therefore, it is not easy to operate; however, it functioned well in space.**Fig. 8** shows the data obtained from the displacement sensor when a circular plug of an electric connector was inserted into a receptacle by twisting the plug. According to the figure, at first, the compliance device was in the neutral position due to the absence of gravity. It shifted –0.8 mm in the x direction due to the pulling force of the tether which is provided against an emergency of floating of the plug during the task. During the insertion of the connector by twisting, the connector was swayed from right to left and from left to right and finally the connection was completed after error compensation of dx =- 0.7 mm and dy = -0.2 mm. The final displacement of dθ=0.4 deg in the θ_Z direction is caused by a residual torque due to the stationary friction arising from the twisted insertion movement.

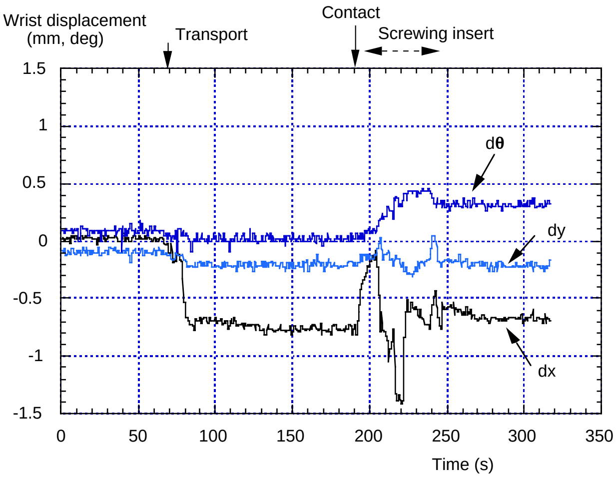

Fig.8 Position error compensation by compliance device in connector screwing insert

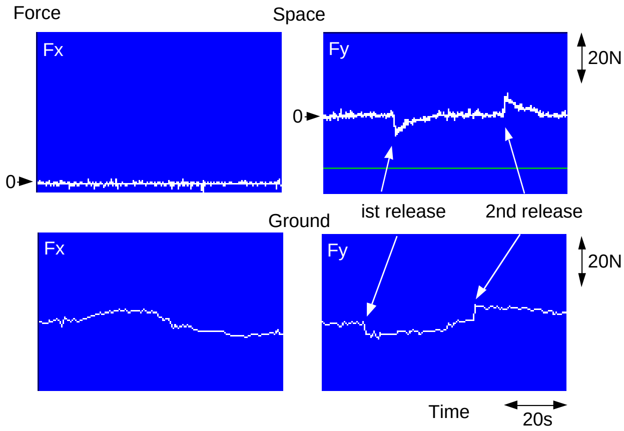

Fig.9 Force-torque sensor data in launch-lock-lever releasing

3.3 Force-torque sensors

A commercially available 6-axes force-torque sensor used for the detection of strain in beams was applied after improvement of its strength and materials so that it can be applied in the space environment. Similar to the testing of the wrist displacement sensor, the tip of the arm was displaced minutely while a fixed workpiece was grasped. The output data were compared with the results obtained by on-ground tests; the agreement between the two results was excellent. The force-torque sensor is not affected by the gravity in orbit, thus in orbit, outputs represent pure action force. **Fig. 9** shows an example of the difference in data obtained in space and that obtained on the ground when launch-lock-levers were pushed down piece by piece by a finger in the ± y directions. The values obtained from the sensor fluctuated due to the weight of the hand itself even during free motion on the ground; the value remains at the zero level until the finger imposes force in space. Furthermore, the force that acts on an object for pushing down maneuvers cannot be determined precisely on the ground; however, the force is clearly applied to the object only in the pushing direction (y) in space. Accordingly, the space is an excellent place for autonomous control using force sensors.

4. Optical sensors

4.1 Proximity range sensor

The triangulation in which a laser beam is targeted onto an object and the reflected beam is received by PSD (Position Sensing Device) was used for range sensors. The measurement range is 0 – 80 mm from the fingertip. When the illuminance is 4,000 lx or greater, it is very difficult to measure distances using commercially available sensors. However, the illuminance on the orbit exceeds

50,000 lx. Therefore, we installed an optical filter with center transmission wavelength of 780 nm and half-value width of 50 nm in front of the PSD. This filter blocked 99.98 % of the sunlight. Also, the analog processing circuit of the sensor exhibits slight nonlinearity and temperature dependence, therefore, the correction using a 2nd order polynomial in terms of temperature was applied to the output voltage, and correction using a 3rd order polynomial in terms of output voltage was applied to the range measurement. These corrections broadened the operating temperature range (-20ºC to +60ºC) in space. **Fig. 10** shows measured range values in the sunlight and in eclipse for the distance between the tip of the finger and an object when the distance was changed by the arm.

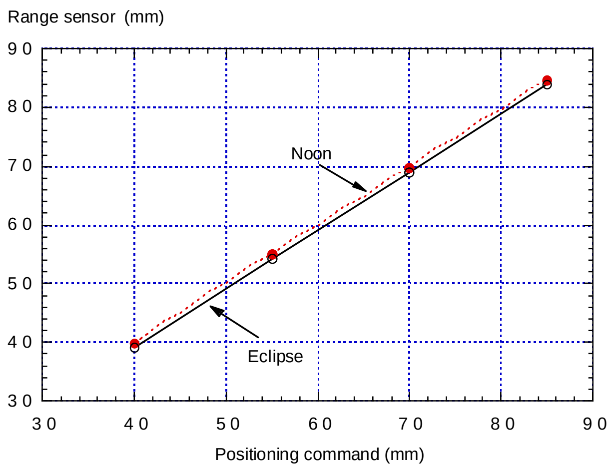

Fig.10 Characteristics of proximity range sensor (in satellite daytime and night)

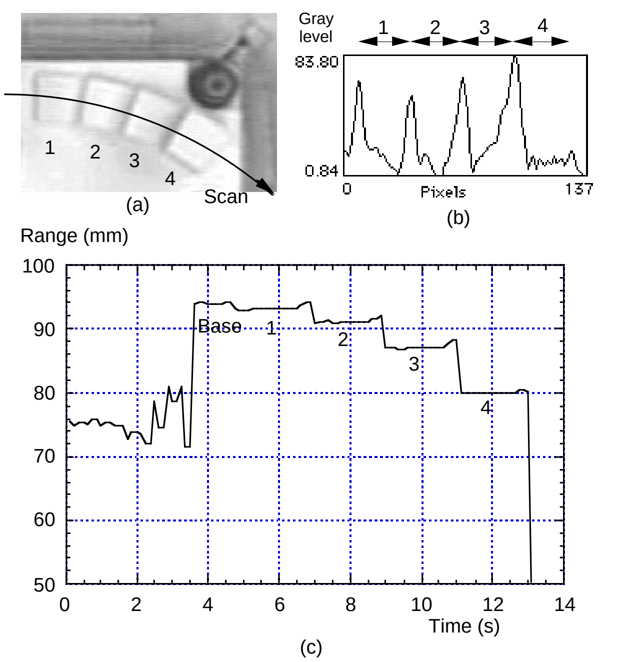

Fig.11 Three-dimensional measurement of steps by scanning range sensor (a: Camera image, b: Density profile of image, c: Range profile)

Measured values in eclipse are approximately 0.5 mm shorter than the values measured in the sunlight. The possible causes of the error may be related to the environmental temperature, illuminance and positioning error of the arm; however, the error values are smaller than the design values, ± 1 mm. Therefore, it does not pose a practical problem.

The range sensor can also be used for measurements of work environment by moving the arm so as to scan the area. **Fig. 11** shows the measurement result of the profile of a step-like object in space. Each step is painted white, and the design values of the heights are 1, 2, 7 and 15 mm from the bottom. (a) shows a camera image of the steps obtained on the ground, (b) shows the density profile of the gray-scale image and (c) shows the range profile. With the range sensor, errors at step border sections are large; however, highly accurate height information is obtained at other locations. On the other hand, the camera image provides the shape of the plane including edge positions at high resolution. By the combined use of (b) and (c), errors are compensated mutually; highly accurate shape data are obtained. Although the range sensor cannot be applied to objects such as mirror-reflected images, it was extremely useful for three-dimensional measurement of objects and for inspecting and evaluating to confirm the completion of work by a robot in orbit where the variation of illuminance is very large.

4.2 Image sensor

A monochromatic CCD camera with 668 x 485 effective pixels was used for the hand-eye camera. The optical view field was set to be 85 x 64 mm at 40 mm from the tip of the finger and a resolution of 0.12 x 0.14 mm was obtained. Eight-bit image signals of a window consisting of 512 pixels and 320 lines are taken into the image memory of the control computer. The illuminance adjustment function is required because the illuminance in orbit changes minute-by-minute depending on the direction of the sun. One red LED array of 1 W is used for local illumination in the eclipse. However, the illuminance by the LED array is approximately 10 lx at 12 cm. The illuminance ratio of sunlight to the LED array light is extremely large; it exceeds the adjustable range of the electronic shutter (1/4 – 1/10,000 sec). Therefore, we used an optical filter to pass only red light. Let the illuminance of sunlight be P_s, the illuminance of the LED array P_l, the transmittivity of sunlight of the optical filter a_s, and the transmittivity of red LED light at, then the illuminance ratio can be obtained as

$$\gamma = \frac{P_s \alpha_s}{P_l \alpha_l} \tag{7}$$

We designed the filter so that the value obtained by Eq. (7) is within the adjustment range of the shutter. Using the filter with center transmission wavelength of 645 nm and half-value width of 30 nm, we can design the filter with as to be $\alpha_s < 0.3$ and $\alpha_l > 0.75$. Accordingly, we were able to arrange the ratio γ to be 2,500 or smaller for P_s =50,000 lx and P_l =8 lx, and set the shutter speed within the adjustable range. **Fig. 12** shows an image of the D-sub connector in sunlight (albedo illumination) and in the eclipse (LED illumination) taken by the camera. The image of objects was satisfactory not only in sunlight but also in the eclipse when 1W LED illumination was used.

In order to evaluate positioning characteristics by the image sensor in orbit, we performed positioning measurement of an 8-mm-diameter black circular mark (1.8 % of the total pixels) on a white board to be suitable for image processing. We succeeded in image processing both in sunlight and in the eclipse. The measurement error was within 0.2 mm; it was sufficiently accurate for practical purposes.

Next, we attempted the measurement of the connector position and its direction from the above image of the pinhole arrangement of the connector. This measurement is performed to determine the connector position and orientation during plugging and unplugging of connectors. The connector used here is a standard item; it is not fabricated by taking the image processing work into consideration. The number of pixels corresponding to each pinhole (diameter: 1.3 mm) is approximately 100 (0.06 % of the total pixels). Measurements were always successful in on-ground tests under fluorescent illumination. However, it is expected that such measurements will be difficult in an environment where the illumination condition varies greatly. **Fig. 13** shows the algorithm used in image measurement. The algorithm is constructed in the following manner; the signals are taken into the image memory and preprocessed, the characteristics of the candidate for the pinhole are extracted sequentially regarding the number of pixels, roundness and density as indices. The conditions of extraction were set as follows; the number of pixels is 14–160, roundness (baseline length for Y)/(baseline length for X) is 0.65–1.05 and the density (pixel number/{(baseline length for Y)*(baseline length of X)}) is 0.6–0.9. When the extracted mutual distance between the labels exceeds the tolerance range of known pitch intervals, the data are excluded as noise. After detecting all pinholes, the distribution of pinholes is approximated by the linear least-squares line, the orientation of the connector is calculated and the center of the connector position is calculated from the centers of gravity of all pinholes. **Table 2** shows the measurement results in sunlight and in the eclipse. Under the two conditions, the difference from the design value is very small; the accuracy of image measurements was good. The accuracy of repeated measurement under the same condition was 0.01 mm or smaller; the reproducibility of data was excellent.

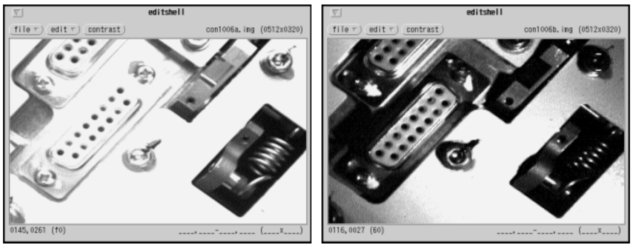

(a) (b)

Fig.12 Image of D-sub receptacle (a: Albedo illumination in satellite daytime, b: LED illumination in eclipse)

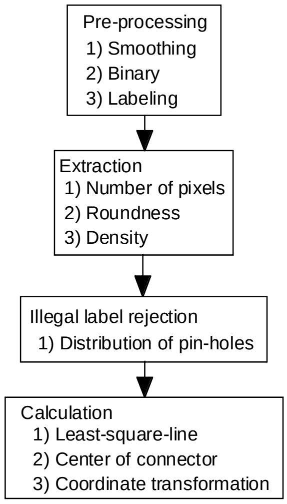

Fig.13 Algorithm of image processing for connector position measurement

Table 2 Connector position measurement by onboard image processing in satellite daytime and night

Condition	Position (x, y) (mm)	Orientation (deg)
Albedo illumination (satellite daytime)	(49.67, 26.67)	-50.48
LED illumination (satellite night)	(49.89, 26.89)	-50.64
Design	(49.00, 26.00)	-50.00

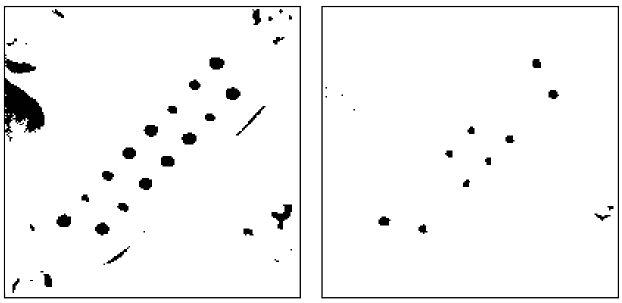

(a) (b)

Fig.14 Binary image of receptacle (a: threshold value=127/256, b: threshold value=81/256)

In the measurements using images under albedo illumination, the number of pins detected was inaccurate and the measurements were not possible in several cases. One of the possible causes of measurement failure is that the adjustment of shutter speed was difficult due to the rapid change in sun illuminance in orbit. According to the downloaded images, the contrast of pins was different from that on the ground obtained under a fluorescent lamp. It is revealed that the extraction condition became insufficient. One of the reasons for this problem was that the number of pixels representing each pin varies greatly due to the fact that the entrance of the hole is acorn-shaped metal. Another reason is the change of reflection characteristics due to the wear of pinhole surface with frequent plugging and unplugging of the connector. **Fig. 14** shows binary images of the receptacle shown in Fig. 12 (a) obtained by setting the threshold values at 127/256 and 81/256. The pinholes, the reflection characteristics of which were altered due to wear due to plugging and unplugging, were not identified at the threshold value of 81/256. Therefore, we suspect that the applicable binary ranges became narrow.

On the other hand, we were successful in the measurement in the eclipse. In the sunlight, even detection of labels was required for the determination of hole density; however, in the eclipse, all pinholes were detected during the evaluation of roundness in the feature extraction process. It is considered that the measurement was successful because the same optical conditions as those obtained on the ground were maintained by the LED illumination in the eclipse; the optimized image processing parameters on the ground were valid even in orbit. Since there is no reflection from surrounding objects during the eclipse, it is a good time period to carry out image measurements.

The following is the summary of information obtained by image measurements; i) We must be careful in image measurements of objects in sunlight for which the pixel number is small and whose optical characteristics are easily affected by the direction of irradiation of light sources. ii) A function to register the shutter speed and the optimal values of image processing parameters in accordance with the position of the sun as a database is desired. iii) The image measurements in the eclipse under LED illumination are extremely effective; it is recommended that measurements be carried out during this time period in cases when external light affects measurements.

4.3 Generation of local coordinate by fusing a range sensor and image sensor

We generated the local coordinates of a work plane by fusing the above-mentioned range sensor and the image sensor. We first obtained a local vertical line (z axis) by controlling the wrist attitude so that the values from three range sensors arranged evenly around the hand become identical. Then we obtained the y axis by taking the image of a unit coordinate mark on the work plane (defined by two circular marks positioned 20 mm apart between the centers) using a hand-eye camera and by image processing. Thus, we generated a local coordinate system (x, y, z) using the marks as the origin. The work plane was painted in white thermal paint and the marks were two 8-mm-diameter black circles to reduce disturbance to the range and image sensors.**Table 3** shows the coordinate elements for the base coordinate system under albedo illumination, LED illumination in the eclipse, and fluorescent lamp illumination on the ground. Under both albedo illumination and in the eclipse, the accuracy of coordinate generation within ±1 mm for positioning and ± 0.2 deg for attitude determination has been realized. This coordinate generation is always successful even under sunlight and we expect that for practical use it will have no problems in space.

Table 3 Coordinate generation by sensor fused measurement using image sensor and range sensors

Condition	Coordinate element			
	x (mm)	z (mm)	(deg)	(deg)
Albedo illumination (satellite daytime)	389.78	434.42	17.10	104.73
LED illunination (eclipse)	389.82	434.37	17.10	104.71
Fluorescent lamp (Ground)	389.25	435.33	17.10	104.57

5. Example of application for precision work in space

We have been performing precision task experiments using the multisensory hand, the performance of which has been proven in the space environment. Here, we describe the practical application of the hand using an example of plugging and unplugging of an electric connector. The connector used in the experiments is the D-sub type which is the most popular for use in space. It is a multiple pin connector, and the guide of the receptacle is narrow; therefore, it is necessary to insert the plug with submillimeter accuracy in terms of the plug position and orientation.

Fig. 15 shows the flow of the control and the utilization of information obtained by the sensors for autonomous execution of the task. As described in the above, the coordinate of the work plane is generated by fusing an image sensor and range sensor, then the image of the connector receptacle is taken using a hand-eye camera and the position and orientation are measured by means of image processing of the pinhole arrangement. The plug approaches the receptacle using the information of the local coordinates. Next, rotating fingers are closed until they touch the plug with the assistance of the grip force sensor, and grasp the plug by closing the linear-motion finger, while controlling the grip force. Then the plug is pulled out and unplugged. Data on a series of movements in space are shown on the upper left of **Fig. 16**. The lower figures show results of on-ground tests. Z represents the vertical distance of the hand from the work plane, and Fz the vertical action force. On the ground, when the hand grasps the plug, Fz decreases due to the release of the weight of the hand itself; however, such a phenomenon does not occur in space. In addition, the force required for unplugging in space was 50% greater than that required on the ground due to the effect of the thermal vacuum environment.

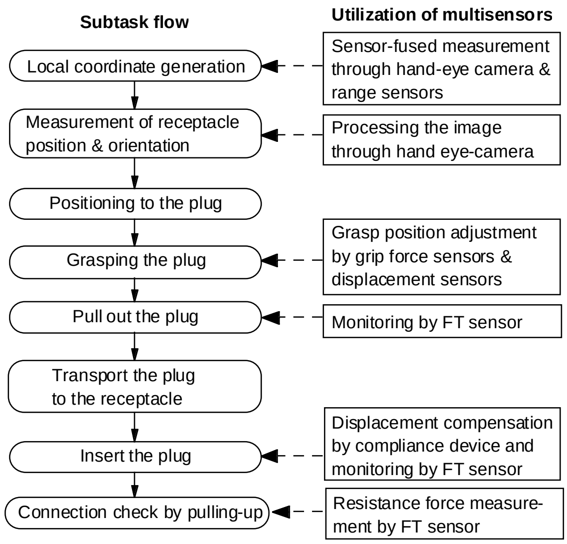

Fig.15 Control flow and multisensory utilization in connector remove/mate task

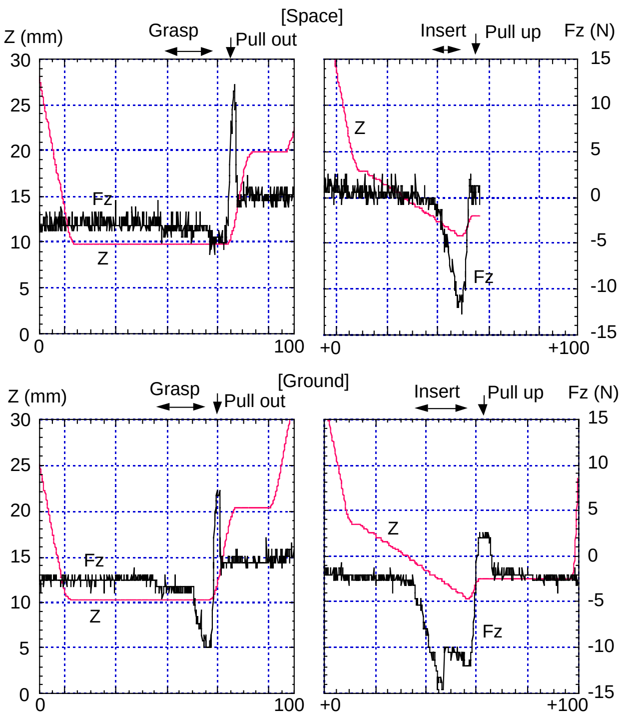

Fig.16 Telemetry data in connector removing and mating (Upper: Space, Lower: Ground)

Next, the removed plug was transported to the position of the receptacle, the location of which is calculated by image measurements, and it was inserted into the receptacle by turning the compliance device on. The mating was confirmed by pulling the plug a minute amount (approx. 2 mm) in the axial direction within the stretch margin of the compliance device, and by detecting the resistance force. This plugging/unplugging task was completed in approximately 20 min by performing divided subtasks using the multisensor-based autonomous control, and operating the sensors in the supervisory mode in which the operation of the arm is monitored on the ground and the operation is proceeded by the Go/No Go command. In these experiments, communications at 4 kbps for commands, 12 kbps for telemetry and 1.2 Mbps for images are established via a data-relay satellite (TDRS) on the geostationary orbit; the communication delay is approximately 5 sec. The autonomous control functioned effectively; precision work was performed under restricted conditions of communication capacity and communication delay. The developed hand was applied to other precision tasks and excellent work performances have been observed[9]. The results of the space experiments including movies can be seen on the web [10].

6. Conclusions

We developed a high-performance hand with newly designed three- finger mechanisms and multiple sensors which are suitable for precision work in space; we installed the hand and arm in the spacevehicle "Hikoboshi," and carried out performance tests in space environments.

Various mechanisms and sensors incorporated in the hand functioned as designed in the severe space environment. The finger mechanism and wrist compliance device, as well as grip force sensors and displacement sensors incorporated into these mechanisms performed the same or better level of operations as they did on the ground when they were operated in space because there were no effects of offsets and disturbance due to the absence of gravity. The laser range sensor and the hand-eye image sensor on the hand functioned as designed in a broad range of optical environments in orbit ranging from sunlight to the eclipse due to the installation of an optical filter. In the field of image-based measurement, it was proven that some caution must be exercised when dealing with images with a small number of pixels and objects having optical characteristics easily affected by the direction of irradiation. In addition, the LED illumination system incorporated in the hand is effective in image-based measurements in the eclipse. The high-accuracy performance of the multisensory hand in orbit was proven using the example of plugging and unplugging of an electrical connector. Furthermore, by the combination of the hand mechanism and multiple sensors, the developed mechanisms and sensors were effective in the measurement of work environment and model calibration.

This is the first time that experiments and evaluations on a multisensory hand have been performed in the space environment; we expect that the obtained data will be important for the practical application of high-performance robots.

Acknowledgment

This project was promoted by METI (Ministry of Economy, Trade and Industry), and flight model was developed by USEF (Institute for Unmanned Space Experiment Free Flyer). The ETS-VII was developed by NASDA. The author thanks the employees of these organizations.

References

1) C. M. Hinds: The Shuttle's Remote Manipulator System - Status and Operation, Advanced Astronaut Sci, 145/157 (1980)
2) H. Borduas, D. Gossain, A. Kong, E. Quittner and D. Shaffer: Concept Design of the Special Purpose Dexterous Manipulator for the Space Station Mobile Servicing System, Canadian Aeronautics and Space Journal, **35**-4, 197/204 (1989)
3) T. Matsueda, F. Kuwano, S. Motohashi and R. Okamura: Development of Japanese Experiment Module Remote Manipulator System, i-SAIRAS 94, 183/186, (1994)
4) M. Oda: Development of the EVA End Effector, Grapple Fixtures and Tools for the Satellite Mounted Robot System, IROS'96, (1996)
5) D. E. Anderson, T. O. Moore, and D. G. James: Hardware Design for Joint EVA and Telerobotic Compatibility, SAE Technical Paper Series, **93**-2222, (1993)
6) G. Hirzinger, B. Brunner, J. Dietrich, and J. Heindel: Sensor-Based Robotics - ROTEX and Its Telerobotic Features, IEEE Trans. on Robotics and Automation, **9**-5, 649/663 (1993)
7) K. Machida, T. Mikami and K. Akita: Development of Precise Telerobotic System for Unmanned Spacecraft, J. of Robotic Society of Japan, **17**-4, 577/586 (1999) (in Japanese)
8) Y.Murase, S. Ishii, S. Komada, K. Machida and K. Akita: Development of 3-finger Multi-Sensory Hand for Space Robot, J. of Robotic Society of Japan,**16**-1,124/133(1998)
9) K. Machida, Y. Toda, H. Nishida, M. Kobayashi, K. Akita: Space Experiment of Advanced Robotic Hand System on ETS-VII, Proc. of 42th Joint Conf. on Space Science and Technology, **98**-1A14, 1/6 (1998)
10) http://www.rosetta.t.u-tokyo.ac.jp/ARH/ARHEng/, (1999)

Kazuo MACHIDA (Member)

Received the M. S. degree in Precision Engineering from Hokkaido University, in 1970. From1970, he worked on the researches of electric propulsion and space robotics at Electrotechnical Laboratory. Since 2002, he has been a professor in Research Center for Advanced Science and Technology at the University of Tokyo.

Yoshitsugu TODA (Member)

Received the M. S. degree in Aeronautic Engineering from Nagoya University, in 1975. Since 1975, he worked on the researches of the ion engine system and space robotics at Electrotechnical Laboratory (AIST).

Yuichi MURASE (Member)

Received the M. S. degree in Mechanical Engineering & Materials Science from Yokohama National University, in 1985. Since 1985, he worked on the researches of space mechanism and robotics in Autonomous System Laboratory at Fujitsu Laboratories Ltd.

Translated from Trans. of the SICE, Vol.35 No.12, 1583/1590 (1999)